Pergamon

Journal of Structural Geology, Vol. 16, No. 7, pp. 997 to 1006, 1994

0191-8141/94 $07.00+0.00

Kinematic behaviour of an interface and competence contrast: analogue models with different degrees of bonding between deformable inclusions and their matrix

F. ODONNE

Laboratoire de Géologie Structurale et Tectonophysique, and URA CNRS No. 67, Université Paul-Sabatier, 38 rue des 36 Ponts, 31400 Toulouse, France

(*Received* 28 *October* 1992; *accepted in revised form* 13 *August* 1993)

Abstract—In a system composed of a ductile matrix with a particle included in it, the deformation of the matrix, the displacement field, and the rotation and the deformation of the block are related to the viscosity ratio between block and matrix and also to the degree of bonding between the matrix and the block. In this paper, belemnites from the Lower Lias of the Alps provide a natural example of moderately deformed objects included in a slaty matrix. They are compared with analogue models made of paraffin, in which a long block of a more competent paraffin is included.

Depending on the degree of bonding between matrix and object, the same block appears to be deformable or quite rigid. With a high degree of bonding, the strain refraction observed corresponds to the viscosity ratio between the block and the matrix. When the degree of bonding is weak, the block is quite undeformed, its rotation is great and the deviation of the strain in the matrix is analogous to that observed around a fault. The kinematic conditions appear to have a greater effect on the finite strain than the viscosity ratio of the materials.

INTRODUCTION

RIGID particles included in a more ductile matrix have been used as kinematic indicators of natural strain in rocks for a long time. The motion of ellipsoidal particles immersed in a viscous fluid is described by Jeffery's (1922) equations. According to these equations, it appears that the motion of the particles is a function of their shape (Cox 1970, Freeman 1985).

Where contact is mechanically weak, the matrix is detached from the object and pressure shadows can develop. The relative particle motion can then be recorded by the growth of fibres (Choukroune 1971, Malavieille *et al.* 1982, Ramsay & Huber 1983, Etchecopar & Malavieille 1987). This motion could also be a function of the degree of bonding between the ductile matrix and the object.

A high degree of bonding, on the other hand, often leads to the deformation of the object. Particles that deform homogeneously with the matrix can be used as strain markers. Initially spherical objects provide strain ellipsoids directly (Cloos 1947). For initially non-spherical objects, the strain ellipsoids are determined by different techniques using lines or angles measured on the deformed objects (Ramsay & Huber 1983).

In a great number of examples, the particles around which pressure shadows develop are not deformed or only slightly so, whereas particles without pressure shadows are deformed along with the matrix. In the first case, the competence contrast between the object and the matrix is thought to be important; in the second, the behaviour is related to the viscosity ratio between the object and the matrix (Ramsay 1982). Detachment and sliding along the interface could be responsible for a great part of this distinction between deformation and non-deformation of the object.

The purpose of this paper is to explore how the kinematic behaviour of an interface influences the effective competence contrast that is observed between an object and its matrix. Moreover, this leads to the question, can a competence contrast always be expressed by a rheological contrast or a viscosity ratio?

In the first part of the paper, deformed belemnites in a slaty matrix provide a natural example in which the competence contrast between deformed fossils and their slaty matrix is moderate. In the second part, an analogue model is used to consider how two parameters: (1) the viscosity ratio between the object and the matrix; and (2) the kinematic behaviour of the interface, affect the deformation of a matrix and inclusions within it.

Many analogue models show the displacement of a rigid or competent body in a ductile matrix and the deformation pattern of the matrix in simple shear (Cox 1971, Bilby & Kolbuszewski 1977, Van den Driessche & Brun 1987), in pure shear (Gay 1968a, Strömgard 1973) or in a combination of pure and simple shear (Ghosh & Ramberg 1976). None of these papers, however, tries to compare the results of two similar models, one where the object is detached from the matrix and one where it is not. Here is an attempt to look at the question of how the interface affects the nature of the finite strain pattern.

COMPETENCE CONTRAST AROUND DEFORMED BELEMNITES

Usually, the objects around which pressure shadows develop are weakly deformed of undeformed, as around

pyrite crystals, for example. In such cases the viscosity ratio between the object and the matrix can be considered as high.

When there are no pressure shadows, the deformation of the matrix cannot be accommodated by displacement along the interface. As a result, the object can deform. Deformed belemnites are well-known strain markers of the Lower Lias sequence of the Alps. Most of the belemnites, being more competent than the matrix, deform heterogeneously by extension across fractures of their skeleton (Badoux 1963, Beach 1979). From measurement of stretched belemnites, the finite strain ellipse can be constructed in the plane of the slaty cleavage, that is the XY plane (Ramsay 1967, Hossain 1979, Ferguson 1981, 1987, Ferguson & Lloyd 1984).

Belemnites lying at a high angle to cleavage also show internal strain (Fig. 1a). The curvature of the cleavage around the tips of the belemnites is proof that the matrix is more ductile than the belemnite during the deformation. Nevertheless, the belemnites are truly deformed. This is clear when comparing the length to width ratio of the belemnite in Fig. 1(a) with the initial ratio of an undeformed belemnite reconstructed from a boudinaged fossil. This ratio is close to 10 for the undeformed fossil, whereas it is about 5 for the belemnite in Fig. 1(a). Pressure solution can be observed in some belemnites (Gratier & Vialon 1980) where the stress concentration induces a dissolution of the fossil itself (Fig. 1b).

Using an analogue model, Ghosh & Sengupta (1973) showed that when the value of the viscosity ratio between the object and the matrix is more than 15, the object does not deform. Thus, according to Ghosh & Sengupta (1973), the viscosity ratio between the belemnite and matrix in Fig. 1(a) should be between 1 (for an object deformed homogeneously with the matrix) and 15 (for an undeformed object). It is difficult to be more precise, however, because the belemnite has not deformed homogeneously. The two tips curve, and there is no cleavage refraction across the belemnite, from which viscosity ratio could be estimated (Treagus 1988). In order to continue the analysis, analogue models have been used. In these models the value of the viscosity ratio was fixed between 1 and 15 and, to investigate the action of the degree of bonding of the interface, the object was attached to the matrix in some experiments and not attached in others.

ANALOGUE MODELS

Slaty cleavage is formed by, and belemnites deformed by, pressure solution, and viscous flow is the rheological behaviour associated with this mechanism (Rutter 1976, Gratier 1987). So, two types of paraffin wax, which is a viscous material (Cobbold 1975, Mancktelow 1988), have been chosen to represent the matrix and the objects in these experiments. In each experiment an elongate inclusion was embedded in a thick layer of paraffin representing the matrix. The model was then deformed by uniaxial shortening.

The analogue materials

The matrix was made of paraffin wax, manufactured by MERCK, with a melting point of 46–48°C. At the temperature of the experiments (30°C) a natural log–log plot of strain rate against stress shows a non-linear viscosity with a stress exponent of 1.8 (Fig. 2). For the same paraffin, but at lower temperatures, Mancktelow (1988) reported an exponent of 2.6. At a temperature of 30°C the material is believed to approach the α–β phase transition, where weakening occurs.

A stiffer paraffin wax was used to represent a more competent object included in the ductile matrix. This is a mixture of two paraffin waxes with different melting points (46–48 and 52–54°C) in the proportion of three parts of the first to one part of the second. At a temperature of 30°C, the stress exponent of this mixture is 3.2. As pressure solution leads to a linear flow law (Rutter 1976), a linear viscous material should ideally have been used in these experiments. However, as this work is mainly focused on the ratio of dynamic viscosities, paraffin wax has been used because it is very easy to obtain a mixture of a special viscosity by mixing two different waxes.

During the experiments, the bulk strain rate was 1.8×10^{-4} s^{-1} and the temperature was 30°C. Imposed on both materials, this strain rate should lead to a dynamic viscosity ratio of about 2 between the mixed paraffin and the 46–48°C paraffin.

In some experiments, silicone grease was introduced between the matrix and the object, to lubricate the interface. This is a non-linear viscous material with a stress exponent of 1.9. The dynamic viscosity ratio between the matrix and the grease is about 600. This is quite enough to create a non-coherent interface around the object.

The experiments

The matrix was made of a large layer of 46–48°C paraffin (70 × 45 × 1.1 cm). A strip of the matrix, 30 × 5 cm in dimensions, was cut out and replaced by an inclusion of mixed paraffin. Elongate inclusions are comparable to belemnites and other semi-rigid inclusions observed in nature. These inclusions were oriented at high angles to a potential cleavage, close to the compression direction. Before deformation, this angle, between the long side of the inclusion and the compression direction, was 30° in most of the experiments.

The model was placed horizontally on a layer of silicone grease in a rectangular box (70 × 60 cm) made of Plexiglass. It was deformed by moving one of the walls of the box (Fig. 3). The displacement of the wall was halted every 5 cm, then the model was cooled and the strain on the surface of the model was measured from small circles drawn before deformation. The complete displacement

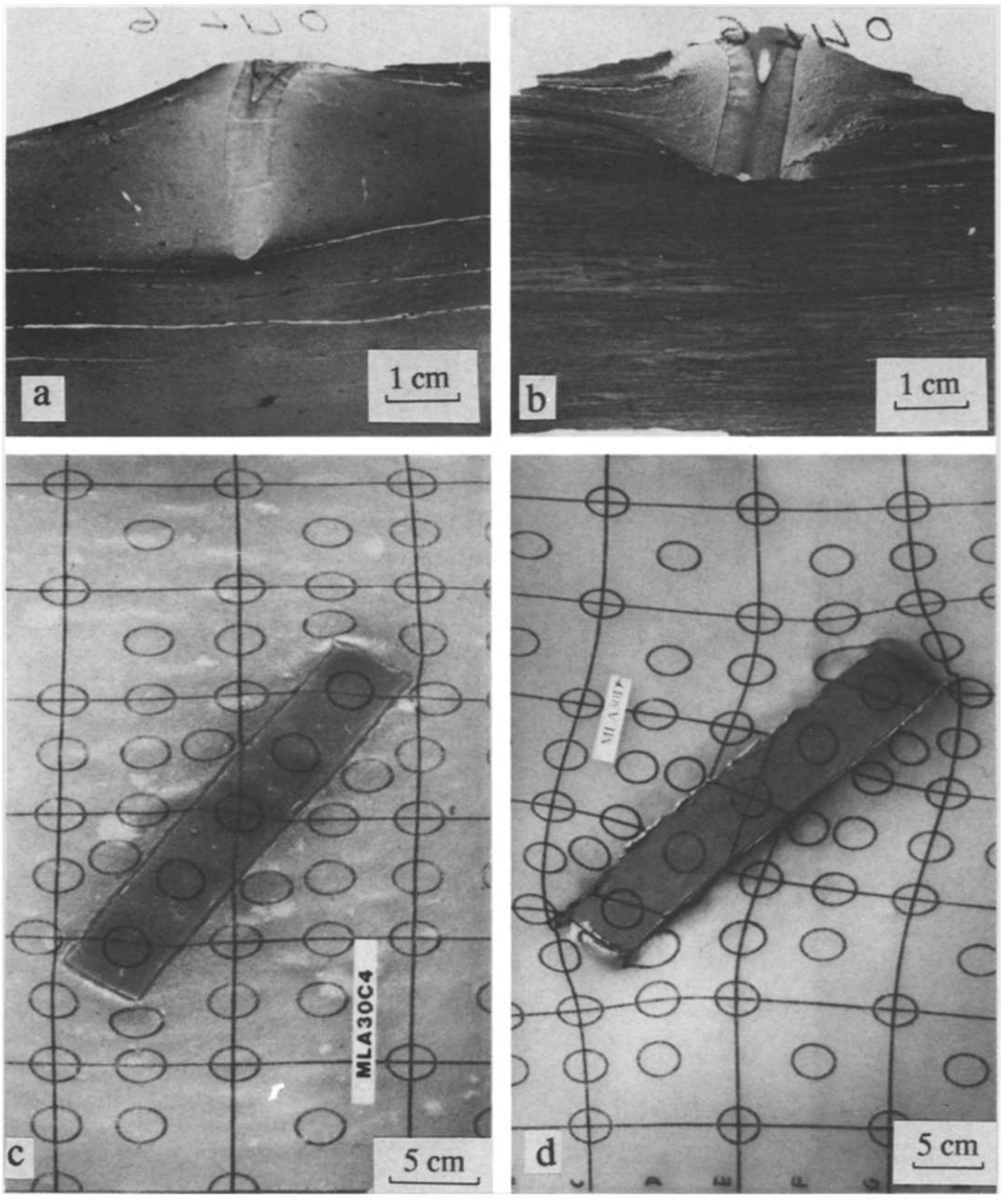

Fig. 1. (a) Thin-section of deformed belemnites from the road to Oulles near Bourg d'Oisans (French Alps). The belemnites lying at a high angle to cleavage are shortened, but they are more competent than the matrix. This is shown by the curvature of the cleavage. (b) A high degree of solution at the tips of some belemnites is proof that pressure solution occurs during deformation. (c) Analogue model made of a competent block of paraffin wax included in more ductile matrix (model 1); a coherent interface of melted paraffin wax joins the matrix and the object. (d) Analogue model in which the interface is not coherent (model 2). The paraffins of the block and the matrix are the same as in the model illustrated in (c).

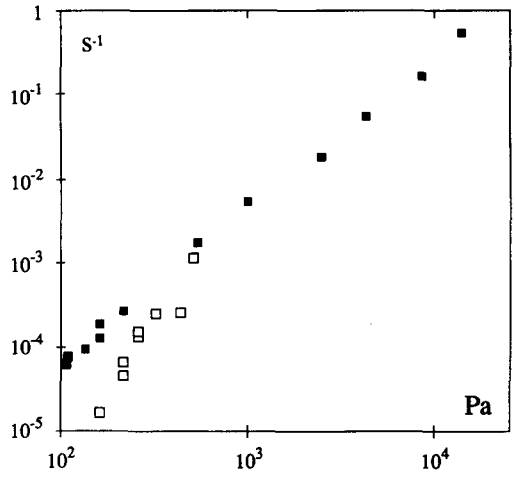

Fig. 2. Natural log–log plot of strain rate (s^{-1}) against stress (Pa) of the 46–48°C paraffin wax (black squares) and mixed paraffin wax (white squares) at a temperature of 30°C. Stress exponents are 1.8 for the 46–48°C paraffin and 3.2 for the mixed paraffin.

of the wall was 20 cm. This corresponds to a finite bulk shortening of 28.5%.

The two complete experiments described in this paper differ only in the nature of the interface. In one experiment (model 1) the matrix and the inclusion were stuck together by melted paraffin (Fig. 1c). In the other (model 2), some grease was introduced at the interface between the matrix and the inclusion to allow sliding (Fig. 1d). Complementary experiments with rigid or short inclusions are described at the end of this paper.

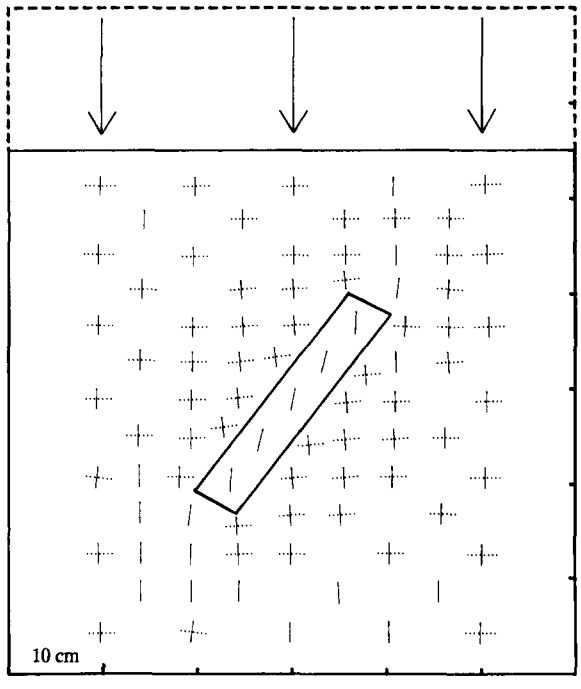

Fig. 3. Map of the finite strain ellipses of model 1 at stage 3 of deformation. The short axes of the ellipses are represented by solid line segments; the long axes are shown with dotted lines if the extension along them exceeds 4%. In this model the competent block of mixed paraffin is stuck to the matrix of 46–48°C paraffin. The block is deformed. A strain refraction can be seen in the model where the finite strain directions deviate in a counterclockwise direction in the matrix and in a clockwise direction in the block.

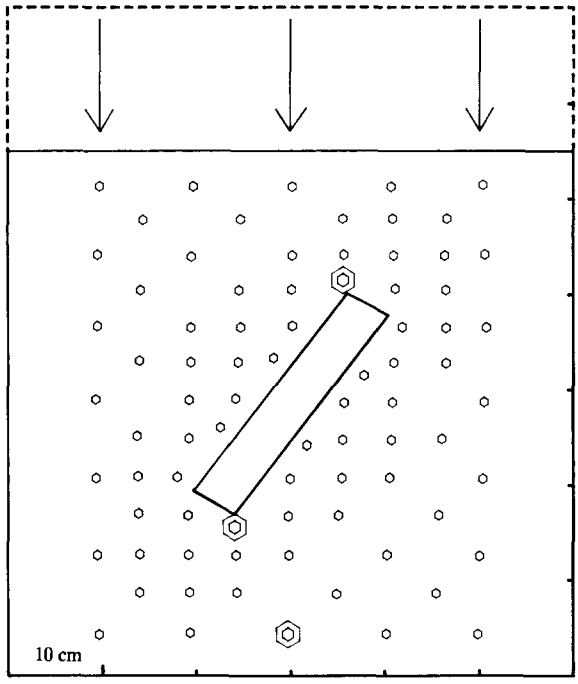

Fig. 4. Comparison of strains at equal distances from the moving wall in model 1, to eliminate strain heterogeneity associated with the wall and friction on the base plate. Horizontal shortening of more than 10% greater than the mean is represented by large concentric hexagons. Values of shortening less than 10% less than the mean do not occur. Two small areas of excess shortening appear at the block tips.

The deformation of the matrix

A deformation map can be drawn at each stage of the experiment. Figure 3 shows this map at stage 3, after the wall displacement reached 15 cm. If we assume that during deformation the volume of paraffin does not change, the change in area of each ellipse is balanced by the vertical thickening of the layer. In the first experiment (model 1), the deformation is not homogeneous. This agrees with the results of Gay (1968b) who demonstrated that a viscous material containing competent objects did not strain homogeneously. Along the long sides of the object, a deviation of the principal axes of strain is observed: this is in a counterclockwise direction in the matrix and in a clockwise direction within the object.

Because a unilateral compression acted on the model, the strain is greater close to the moving wall. For a better understanding of the heterogeneous strain introduced by the object, we have to eliminate the influence of the moving wall. Ellipses equidistant from the moving wall are compared. A mean value of the length of the short axes of finite strain ellipses in each group is calculated, then each ellipse compared with the mean of its group. If the shortening differs by more than 10% from the mean, the size of the small hexagon that represents each ellipse in Fig. 4 is changed. Two large concentric hexagons are drawn if the shortening is greater than the mean, and a large dotted hexagon if the shortening is less than the mean (Fig. 4). The heterogeneity introduced in the deformation of the matrix in model 1 is minimal, only

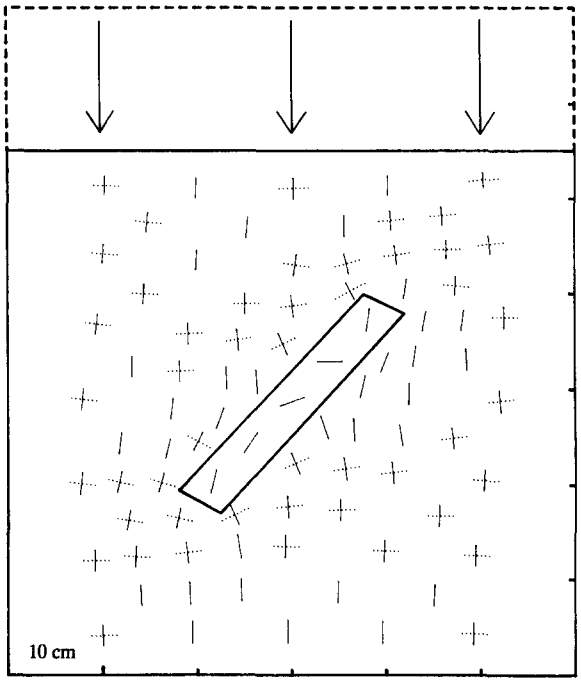

Fig. 5. Map of the finite strain ellipses of model 2 at stage 3 of the deformation. The materials are the same as in model 1, and the interface is non-coherent. The block is quite undeformed and deformation is very heterogeneous in the matrix. Along one side of the block, the deviation of strain is in a clockwise direction at one tip, while it is counterclockwise at the other tip, as along a fault.

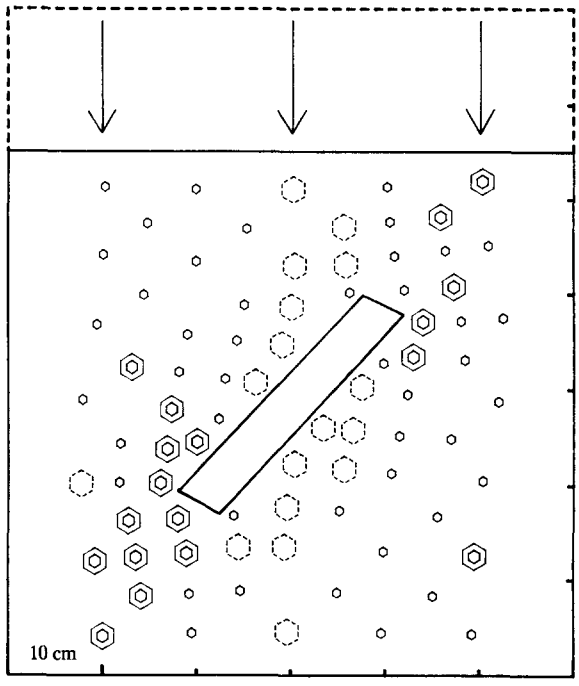

Fig. 6. Comparison of strains at equal distances from the moving wall in model 2. Horizontal shortening of more than 10% greater than the mean is represented by large concentric hexagons, and horizontal shortening of less than 10% less than the mean is represented by dotted hexagons. Shortening appears to be concentrated at the tips of the object where the matrix is displaced to after sliding along the interface.

the ellipses located at the corners of the block are unusually deformed.

In model 2 the matrix was detached from the object, silicone grease on the interface preventing the matrix and the object from sticking together. The deformation map is drawn at stage 3 of the experiment (Fig. 5). The strain is very heterogeneous and is not, unlike in the previous experiment, a result of strain refraction only. The deviation of the strain ellipses along one side of the block is not homogeneous: it is observed to be in a clockwise direction at one tip of the block, whereas it is counterclockwise at the other tip. This deviation of the principal directions of strain is the same as that observed around large faults (Anderson 1951, Chinnery 1963) or small fractures (Segall & Pollard 1980, Gamond 1983).

The heterogeneity of strain is shown in Fig. 6, where the lengths of the short axes are compared. Here, the more shortened ellipses are not located between the object and the compressing wall, as in model 1 (Fig. 4), but at the tips of the object where the matrix is displaced after sliding along the object. This organization of the compressed areas is the same as along a fault (Odonne 1990).

The deformation of the blocks

In both analogue models, the blocks are deformed, but not in exactly the same way (Fig. 1). In model 1, the block is less deformed than the matrix and a strain refraction can be observed all along the object (Fig. 3). Treagus (1981) has shown that, between two adjacent layers, a strain refraction is related to a viscosity contrast. The strain pattern that can be observed around an elongate object appears to be similar to that produced by a layer embedded in a viscous matrix. It can be seen that this strain refraction is produced by a very small viscosity contrast; in this experiment the viscosity ratio between the matrix and the object is about 2.

In model 2, where the matrix is detached from the object, the deviation of the strain inside the block appears to be unorganized. In fact, the strain ellipses within the object are almost undeformed (Fig. 1d). At stage 3 of the experiment, the mean value of the short axes of these finite strain ellipses $(1 + e_2)$ is 0.93, while it is 0.85 in the block of model 1. The scattering of the orientations reflects more the difficulty in measuring than the organization of the deformation. Because dynamic viscosity is a relation between stress and strain rate, it is difficult to be sure of the viscosity ratio in this second experiment in which the stresses are not completely transmitted in the block when a sliding occurs on the interface.

An important result of these experiments is that two inclusions made of the same material appear to be either deformed or quite undeformed according to the degree of bonding at the interface. The block is quite undeformed if displacement is possible along the interface, and deformed if displacement is impossible. Strömgard (1973) has already emphasized a similar difference in the deformation of boudins according to the degree of cohesion across the contacts between the boudins and

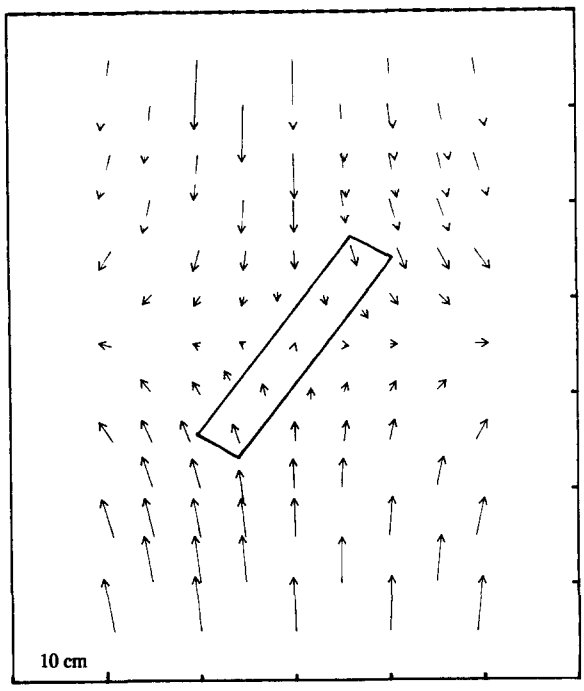

Fig. 7. Displacement vectors relative to the centre of the block of model 1. They show a displacement field analogous to that of a pure shear. Rotation of the block during the experiment is not large and is associated with a shortening of the long sides.

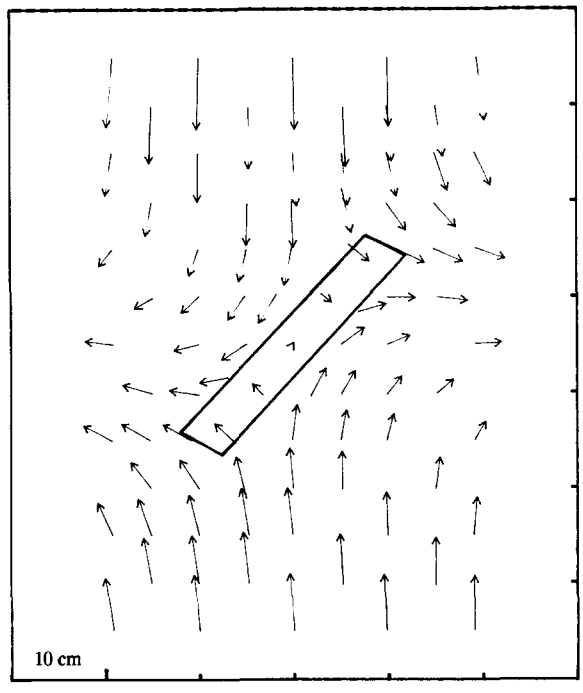

Fig. 8. Displacement vectors relative to the centre of the block of model 2. They exhibit a left-lateral displacement along the interface and rotation of the block in a clockwise direction. A very small shortening is recorded by the block during the experiment.

the matrix. During folding, a similar influence is known: analogue experiments show that the rate of fold propagation may be influenced by the degree of bonding between layer and matrix (Abbassi & Mancktelow 1990).

Displacement field and rotation of the blocks

The displacement vector fields drawn between the undeformed state and stage 3 of each experiment show two types of displacement field. In model 1, the displacement vectors relative to the centre of the model show a N–S shortening and an E–W stretching (Fig. 7). This displacement field is similar to that of a pure shear deformation (Ramsay & Huber 1983), but it is not a pure shear because of the non-plane strain conditions of these experiments. In model 2, the displacement field is more complex (Fig. 8). The shortening direction is still N–S but the stretching direction is not exactly E–W. Left-lateral displacement along the block introduces a non-coaxial strain history, the result of which is a significant rotation of the block.

Under unilateral compression, the blocks rotate toward the direction of the flattening plane, as they do in pure shear (Gay 1968a). This rotation is greater in model 2 where the object is detached from its matrix (Fig. 9). Rotation is 20° at the end of the experiment in this model, while it is only 11° in model 1.

In model 2, the block rotates easily, allowing it to escape from the compression direction, and this block is less deformed than that in model 1. In model 2, however, the deformation of the matrix is very different from the deformation of the object. The rotation of the block appears to be a means of accommodating the heterogeneous strain in the model.

Some further data provided by experiments with rigid objects

Several experiments have also been done with square, rigid or segmented blocks. The most interesting results are supplied by models with rigid blocks. In these experiments a block made of 52–54°C paraffin, which is still rigid at 30°C, was substituted for the block made of mixed paraffin from the previous experiments. In three experiments with rigid blocks with a coherent interface, differing only in the shape of the block, there are deviations in the finite strain directions along the sides of the blocks. The shape of the block, square (Fig. 10), rectangular (Fig. 11) or elongate (Fig. 12) does not seem to influence the amount of deviation, unlike the strain concentration, which is greatest at the tips of the elongate block and noticeably less around the square and rectangular blocks. Of course, the rotation of the block is dependent on its shape. During the deformation (28.5% finite bulk shortening), the rotation of the elongate block is 8°; it is 6° for the rectangular block and zero for the square block.

Lastly, an experiment with an elongate rigid block detached from its matrix has been carried out (Fig. 13). The rotation of the block is very easy, being 14° at the end of the experiment. The deviation of the principal directions of the strain ellipses along the block is the same as around a fault or around a non-rigid block detached from its matrix (Fig. 5).

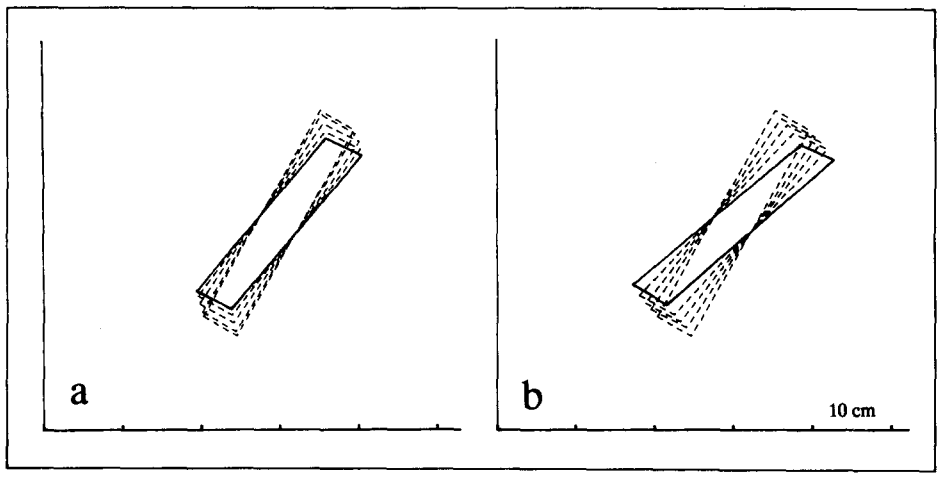

Fig. 9. Rotation and strain of the blocks in (a) model 1 and (b) model 2. The successive positions of each block are superimposed on the positions at the end of deformation. (a) When there is a high degree of bonding between block and matrix, the block is shortened and does not rotate much. (b) When the interface is non-coherent, rotation is large while deformation of the block is small.

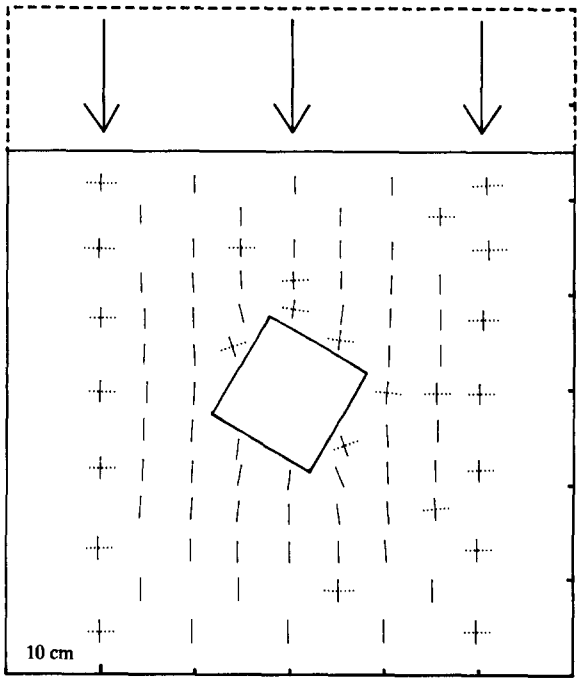

Fig. 10. Map of the finite strain ellipses of a model with a rigid square block at stage 3 of deformation. In this model, the block is made of 52–54°C paraffin and is separated from the matrix (made of 46–48°C paraffin) by a coherent interface. The deformation pattern in the matrix is not very heterogeneous.

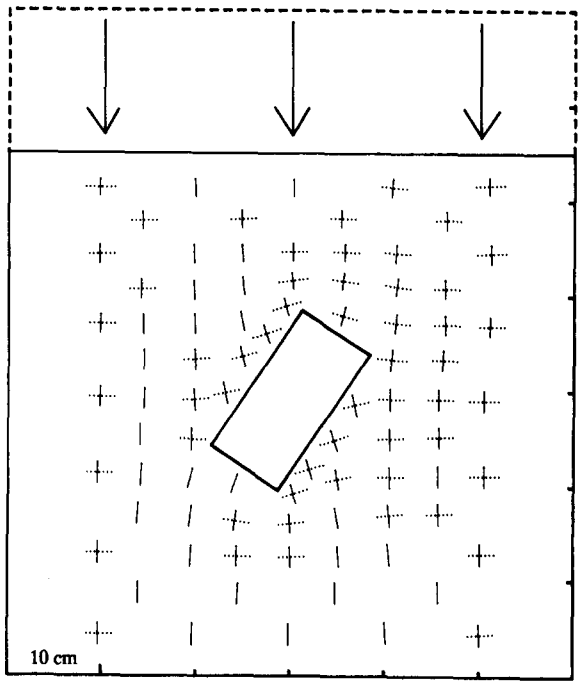

Fig. 11. Map of the finite strain ellipses of a model with a rigid rectangular block at stage 3 of deformation. The materials are the same as in the experiment illustrated in Fig. 10. The interface is coherent. In the matrix, the finite strain directions deviate in counter-clockwise and clockwise directions along the long and short sides of the block, respectively.

DISCUSSION

Borradaile (1981) showed that cleavage planes deflected around a rigid object give a measurement of strain. However, this technique provides only first-order-of-accuracy of strain intensity and generally gives a minimum value. As demonstrated by Cobbold & Barbotin (1988), the curvature of a strain trajectory does not always imply an increase in strain intensity. In the experiments that are presented here, the curvature of the flattening plane around competent bodies does not correspond systematically to the point of highest strain. In Fig. 6, the ellipses that are most shortened (indicated by concentric hexagons) are not located in the areas of highest curvature of the flattening plane (Fig. 5).

Another result from these experiments is that, in two experiments with the same bulk shortening, the curvature of the flattening planes differs according to the degree of bonding between matrix and object. Where displacement at the interface is large, the curvature is considerable (Fig. 5), but where the interface is coherent, the curvature is slight (Fig. 3). This emphasizes the importance of interface behaviour.

Only when the interface is coherent is strain refraction related to the viscosity ratio (Treagus 1981, 1983, Cobbold 1983, Treagus & Sokoutis 1992). It has been

demonstrated theoretically (Treagus 1981) that competent layers exhibit relatively low strain and strain axes lie approximately orthogonal to layering with a non-coaxial strain history (Treagus 1988). This is why, in the block of model 1, the strain axes deviate from the shortening direction and are parallel to the long axis of the block (Fig. 3). When the contact is mechanically weak, on the other hand, as in model 2, the matrix is detached from the object and the displacement field is more complex than in model 1. In natural examples, pressure shadows record these displacements (Passchier & Simpson 1986, Etchecopar & Malavieille 1987, Bell *et al.* 1989). The analogue model also shows that an important consequence of the detachment is that whatever the characteristics of the block, it appears rigid during deformation when the degree of bonding between matrix and object is weak. In this case, as the stresses are not completely transmitted into the block, it is difficult to be sure of the viscosity ratio.

To conclude, these analogue models show that kinematic conditions appear to have a greater action on the finite strain pattern than the viscosity ratio or the shape of the different parts of the structure. If an easy displacement is possible in the material, the deformation is organized around the kinematic discontinuity. The heterogeneous strain due to different materials with ductility contrasts depends primarily on the kinematic conditions.

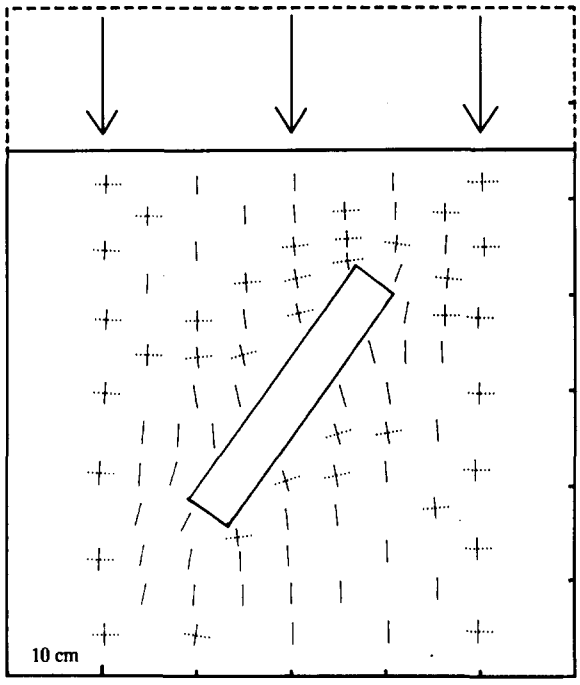

Fig. 12. Map of the finite strain ellipses of a model with a rigid elongate block at stage 3 of deformation. In this model, the interface is coherent. The deformation in the matrix is concentrated around the tips of the block. The deviation of the finite strain directions is analogous to that of the rectangular block (Fig. 11).

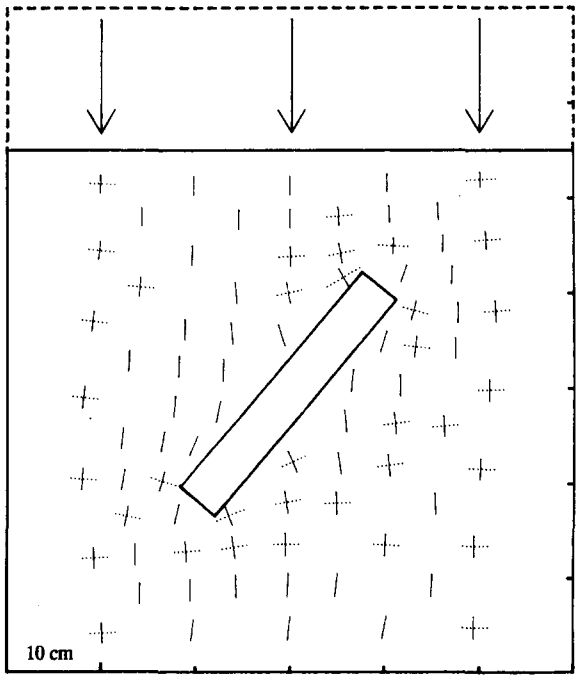

Fig. 13. Map of the finite strain ellipses of a model with a rigid elongate block at stage 3 of deformation. This experiment is the same as the one illustrated in Fig. 12, but with a non-coherent interface. The deformation pattern in the matrix is the same as for model 2 (non-coherent interface around a deformable block). Compare this figure with Fig. 5.

Acknowledgements—I thank the Société Nationale ELF Aquitaine (Production) who have financed this research programme and permitted publication. I am very grateful to Mr. P. Janot who instigated this work. I am grateful both to Peter Hudleston and to the two reviewers of this paper for their constructive advice and criticisms.

REFERENCES

Abbassi, M. R. & Mancktelow, N. S. 1990. The effect of initial perturbation shape and symmetry on fold development. *J. Struct. Geol.* **12**, 273–282.

Anderson, E. M. 1951. *The Dynamics of Faulting*. Oliver and Boyd, Edinburgh.

Badoux, H. 1963. Les bélemnites tronçonnées de Leytron (Valais). *Bull. Lab. Géol. Min. Géoph. Musée Géol. Univ. Lausanne* **138**, 1–7.

Beach, A. 1979. The analysis of deformed belemnites. *J. Struct. Geol.* **1**, 127–135.

Bell, T. H., Duncan, A. C. & Simmons, J. V. 1989. Deformation partitioning, shear zone development and the role of undeformable objects. *Tectonophysics* **158**, 163–171.

Bilby, B. A. & Kolbuszewski, M. L. 1977. The finite deformation of an inhomogeneity in two-dimensional slow viscous incompressible flow. *Proc. R. Soc. Lond.* **A355**, 335–353.

Borradaile, G. J. 1981. Minimum strain from conglomerates with ductility contrast. *J. Struct. Geol.* **3**, 295–297.

Chinnery, M. A. 1963. The stress changes that accompany strike-slip faulting. *Bull. seism. Soc. Am.* **53**, 921–932.

Choukroune, P. 1971. Contribution à l'étude des mécanismes de la déformation avec schistosité grâce aux cristallisations syncinématiques dans les "zones abritées" ("pressure shadows"). *Bull. Soc. géol. Fr.* **7**, 257–271.

Cloos, E. 1947. Oolite deformation in the South Mountain Fold, Maryland. *Bull. geol. Soc. Am.* **58**, 843–918.

Cobbold, P. R. 1975. Fold propagation in single embedded layers. *Tectonophysics* **27**, 333–351.

Cobbold, P. R. 1983. Kinematic and mechanical discontinuity at a coherent interface. *J. Struct. Geol.* **5**, 341–349.

Cobbold, P. R. & Barbotin, E. 1988. The geometrical significance of strain trajectory curvature. *J. Struct. Geol.* **10**, 211–218.

Cox, R. G. 1970. The motion of long slender bodies in a viscous fluid. Part 1. General theory. *J. Fluid Mech.* **44**, 791–810.

Cox, R. G. 1971. The motion of long slender bodies in a viscous fluid. Part 2. Shear flow. *J. Fluid. Mech.* **45**, 625–657.

Etchecopar, A. & Malavieille, J. 1987. Computer models of pressure shadows: a method for strain measurements and shear-sense determination. *J. Struct. Geol.* **9**, 667–677.

Ferguson, C. C. 1981. A strain reversal method for estimating extension from fragmented rigid inclusions. *Tectonophysics* **79**, T43–T52.

Ferguson, C. C. 1987. Fraction and separation histories of stretched belemnites and other rigid-brittle inclusions in tectonites. *Tectonophysics* **139**, 255–273.

Ferguson, C. C. & Lloyd, G. E. 1984. Extension analysis of stretched belemnites: a comparison of methods. *Tectonophysics* **101**, 199–206.

Freeman, B. 1985. The motion of rigid ellipsoidal particles in slow flows. *Tectonophysics* **113**, 163–183.

Gamond, J. F. 1983. Displacement features associated with fault zones: a comparison between observed examples and experimental models. *J. Struct. Geol.* **5**, 33–45.

Gay, N. C. 1968a. The motion of rigid particles embedded in a viscous fluid during pure shear deformation of the fluid. *Tectonophysics* **5**, 81–88.

Gay, N. C. 1968b. Pure shear and simple deformation of inhomogeneous viscous fluids. 1. Theory. *Tectonophysics* **5**, 211–234.

Ghosh, S. K. & Ramberg, H. 1976. Reorientation of inclusions by combination of pure shear and simple shear. *Tectonophysics* **34**, 1–70.

Ghosh, S. K. & Sengupta, S. 1973. Compression and simple shear of test models with rigid and deformable inclusions. *Tectonophysics* **17**, 133–175.

Gratier, J. P. 1987. Pressure solution-deposition creep and associated tectonic differentiation in sedimentary rocks. In: *Deformation of Sediments and Sedimentary Rocks*, (edited by Jones, M. E. & Preston, R. M. F.). *Spec. Publs geol. Soc. Lond.* **29**, 25–38.

Gratier, J. P. & Vialon, P. 1980. Deformation pattern in a heterogeneous material: Folded and cleaved sedimentary cover immediately overlying a crystalline basement. (Oisans, French Alps). *Tectonophysics* **65**, 151–160.

Hossain, K. M. 1979. Determination of strain from stretched belemnites. *Tectonophysics* **60**, 279–288.

Jeffery, G. B. 1922. The motion of ellipsoidal particles immersed in a viscous fluid. *Proc. R. Soc. Lond.* **102**, 161–179.

Malavieille, J., Etchecopar, A. & Burg, J. P. 1982. Analyse de la géométrie des zones abritées: simulation et application à des exemples naturels. *C. r. Acad. Sci. Paris* **294**, 279–284.

Mancktelow, N. S. 1988. The rheology of paraffin wax and its usefulness as an analogue for rocks. *Bull. Geol. Inst. Univ. Uppsala* **14**, 181–193.

Odonne, F. 1990. The control of deformation intensity around a fault: natural and experimental examples. *J. Struct. Geol.* **12**, 911–921.

Passchier, C. W. & Simpson, C. 1986. Porphyroclast systems as kinematic indicators. *J. Struct. Geol.* **8**, 831–843.

Ramsay, J. G. 1967. *Folding and Fracturing of Rocks*. McGraw-Hill, New York.

Ramsay J. G. 1982. Rock ductility and its influence on the development of tectonic structures in mountain belts. In: *Mountain Building Processes* (edited by Hsü, K. J.). Academic Press, London, 111–127.

Ramsay, J. G. & Huber, M. I. 1983. *The Techniques of Modern Structural Geology, Volume* 1: *Strain Analysis*. Academic Press, London.

Rutter, E. H. 1976. The kinetics of rock deformation by pressure-solution. *Phil. Trans. R. Soc. Lond.* **A283**, 43–54.

Segall, P. & Pollard, D. D. 1980. Mechanics of discontinuous faults. *J. geophys. Res.* **85**, 4337–4350.

Strömgard, K. E. 1973. Stress distribution during formation of boudinage and pressure shadows. *Tectonophysics* **16**, 215–248.

Treagus, S. H. 1981. A theory of stress and strain variations in viscous layers, and its geological implications. *Tectonophysics* **72**, 75–103.

Treagus, S. H. 1983. A theory of finite strain variation through contrasting layers, and its bearing on cleavage refraction. *J. Struct. Geol.* **5**, 351–368.

Treagus, S. H. 1988. Strain refraction in layered systems. *J. Struct. Geol.* **10**, 517–527.

Treagus, S. H. & Soukoutis, D. 1992. Laboratory modelling of strain variation across rheological boundaries. *J. Struct. Geol.* **14**, 405–424.

Van den Driessche, J. & Brun, J. P. 1987. Rolling structures at large shear strain. *J. Struct. Geol.* **9**, 691–704.